Appendix 1

Theory of isotopic exchange

1. The five types of exchange model

In order to fit the experimental data obtained during the experiment with H/D isotopic exchange between methane and a proton-conducting oxide, it is necessary to obtain analytical solutions for *Y* variables and concentrations of methane isotopomers. These analytical solutions can be obtained if we find the dependence of the deuterium fraction among the methane isotopomers in the gas phase with time.

The time dependence of the deuterium fraction in the gas phase can be described by solving differential equation (11), taking into account equation (25), as follows:

$$\delta = \gamma + (\delta^0 - \gamma)e^{-r_H(1+\lambda)\tau}, \tag{1 A1}$$

where δ^0 represents an initial deuterium fraction in the gas phase; γ is an equilibrium deuterium fraction in the gas phase and the solid; and λ corresponds to the ratio of exchanged atoms between the gas phase and the solid. This equation, called the exponential kinetic model, represents the boundary case of heterogeneous exchange, when the heterogeneous exchange with the surface is the limiting stage of the exchange. Thus, equation (1 A1) is applicable only for powder samples where hydrogen diffusion is fast enough to be neglected in the calculation.

In the case of exponential kinetics, the general solution of differential equations (18)–(22) can be found with the following boundary conditions: if $\tau = 0$, then $\delta = \delta^0$ and $Y_i = Y_i^0$. On account of the fact that differential equations (18)–(22) are first-order differential equations, an analytical solution of the equations can be presented as the following:

$$\begin{aligned} Y_{CH4} = \Bigg(\Bigg(& -\frac{\big((4\lambda-8)r_4+(\lambda-5)r_3-2r_2\big)(\delta^0-\gamma)(\gamma-1)e^{-\frac{3}{4}\left((r_1+2r_2+3r_3+4r_4)\lambda-\frac{1}{3}(4r_0+r_1-2r_2-5r_3-8r_4)\right)\tau}}{-\frac{3}{4}(r_1+2r_2+3r_3+4r_4)\lambda+r_0+\frac{1}{4}(r_1-2r_2-5r_3-8r_4)} \\ & +\frac{(\gamma-1)^2 r'' e^{-\frac{1}{2}((r_1+2r_2+3r_3+4r_4)\lambda-2r_0-r_1+r_3+2r_4)\tau}}{-\frac{1}{2}(r_1+2r_2+3r_3+4r_4)\lambda+r_0+\frac{1}{2}(r_1-r_3-2r_4)} \\ & +\frac{\big((\lambda^2-2\lambda+3)r_4+(-\lambda+2)r_3+r_2\big)(\delta^0-\gamma)^2 e^{-((r_1+2r_2+3r_3+4r_4)\lambda-r_0+r_2+2r_3+3r_4)\tau}}{-(r_1+2r_2+3r_3+4r_4)\lambda+r_0-r_2-2r_3-3r_4}\Bigg)(\delta^0-\gamma)^2(1+\lambda)^2 \\ & -\Bigg(-\frac{\big((4\lambda-8)r_4+(\lambda-5)r_3-2r_2\big)(\delta^0-\gamma)(\gamma-1)}{-\frac{3}{4}(r_1+2r_2+3r_3+4r_4)\lambda+r_0+\frac{1}{4}(r_1-2r_2-5r_3-8r_4)} \\ & +\frac{(\gamma-1)^2 r''}{-\frac{1}{2}(r_1+2r_2+3r_3+4r_4)\lambda+r_0+\frac{1}{2}(r_1-r_3-2r_4)}+\frac{\big((\lambda^2-2\lambda+3)r_4+(-\lambda+2)r_3+r_2\big)(\delta^0-\gamma)^2}{-(r_1+2r_2+3r_3+4r_4)\lambda+r_0-r_2-2r_3-3r_4}\Bigg)(\delta^0-\gamma)^2(1 \\ & +\lambda)^2+Y_{CH4}^0\Bigg)e^{-r\tau} \end{aligned} \tag{2 A1}$$

$$\begin{aligned} Y_{CH3D} = \Bigg(\Bigg(& -\frac{1}{4}\frac{\big((4\lambda-8)r_4+(\lambda-5)r_3-2r_2\big)(\delta^0-\gamma)(4\gamma-3)e^{-\frac{3}{4}\left((r_1+2r_2+3r_3+4r_4)\lambda-\frac{1}{3}(4r_0+r_1-2r_2-5r_3-8r_4)\right)\tau}}{-\frac{3}{4}(r_1+2r_2+3r_3+4r_4)\lambda+r_0+\frac{1}{4}(r_1-2r_2-5r_3-8r_4)} \\ & +\frac{1}{2}\frac{(2\gamma-1)(\gamma-1)r'' e^{-\frac{1}{2}((r_1+2r_2+3r_3+4r_4)\lambda-2r_0-r_1+r_3+2r_4)\tau}}{-\frac{1}{2}(r_1+2r_2+3r_3+4r_4)\lambda+r_0+\frac{1}{2}(r_1-r_3-2r_4)} \\ & +\frac{\big((\lambda^2-2\lambda+3)r_4+(-\lambda+2)r_3+r_2\big)(\delta^0-\gamma)^2 e^{-((r_1+2r_2+3r_3+4r_4)\lambda-r_0+r_2+2r_3+3r_4)\tau}}{-(r_1+2r_2+3r_3+4r_4)\lambda+r_0-r_2-2r_3-3r_4}\Bigg)4(\delta^0-\gamma)^2(1+\lambda)^2 \\ & -\Bigg(-\frac{1}{4}\frac{\big((4\lambda-8)r_4+(\lambda-5)r_3-2r_2\big)(\delta^0-\gamma)(4\gamma-3)}{-\frac{3}{4}(r_1+2r_2+3r_3+4r_4)\lambda+r_0+\frac{1}{4}(r_1-2r_2-5r_3-8r_4)} \\ & +\frac{1}{2}\frac{(2\gamma-1)(\gamma-1)r''}{-\frac{1}{2}(r_1+2r_2+3r_3+4r_4)\lambda+r_0+\frac{1}{2}(r_1-r_3-2r_4)}+\frac{\big((\lambda^2-2\lambda+3)r_4+(-\lambda+2)r_3+r_2\big)(\delta^0-\gamma)^2}{-(r_1+2r_2+3r_3+4r_4)\lambda+r_0-r_2-2r_3-3r_4}\Bigg)4(\delta^0 \\ & -\gamma)^2(1+\lambda)^2+Y_{CH3D}^0\Bigg)e^{-r\tau} \end{aligned} \tag{3 A1}$$

$$Y_{CH2D2} = \left(-\left(-\frac{1}{2}\frac{\left((4\lambda-8)r_4+(\lambda-5)r_3-2r_2\right)(\delta^0-\gamma)(2\gamma-1)e^{-\frac{3}{4}\left((r_1+2r_2+3r_3+4r_4)\lambda-\frac{1}{3}(4r_0+r_1-2r_2-5r_3-8r_4)\right)\tau}}{-\frac{3}{4}(r_1+2r_2+3r_3+4r_4)\lambda+r_0+\frac{1}{4}(r_1-2r_2-5r_3-8r_4)} \right.\right. \quad (4\ A1)$$

$$\left. + \frac{1}{6}\frac{(6\gamma^2-6\gamma+1)r''e^{-\frac{1}{2}((r_1+2r_2+3r_3+4r_4)\lambda-2r_0-r_1+r_3+2r_4)\tau}}{-\frac{1}{2}(r_1+2r_2+3r_3+4r_4)\lambda+r_0+\frac{1}{2}(r_1-r_3-2r_4)} \right.$$

$$\left. + \frac{\left((\lambda^2-2\lambda+3)r_4+(-\lambda+2)r_3+r_2\right)(\delta^0-\gamma)^2e^{-((r_1+2r_2+3r_3+4r_4)\lambda-r_0+r_2+2r_3+3r_4)\tau}}{-(r_1+2r_2+3r_3+4r_4)\lambda+r_0-r_2-2r_3-3r_4} \right) 6(\delta^0-\gamma)^2(1+\lambda)^2$$

$$+\left(-\frac{1}{2}\frac{\left((4\lambda-8)r_4+(\lambda-5)r_3-2r_2\right)(\delta^0-\gamma)(2\gamma-1)}{-\frac{3}{4}(r_1+2r_2+3r_3+4r_4)\lambda+r_0+\frac{1}{4}(r_1-2r_2-5r_3-8r_4)} \right.$$

$$\left. + \frac{1}{6}\frac{(6\gamma^2-6\gamma+1)r''}{-\frac{1}{2}(r_1+2r_2+3r_3+4r_4)\lambda+r_0+\frac{1}{2}(r_1-r_3-2r_4)} + \frac{\left((\lambda^2-2\lambda+3)r_4+(-\lambda+2)r_3+r_2\right)(\delta^0-\gamma)^2}{-(r_1+2r_2+3r_3+4r_4)\lambda+r_0-r_2-2r_3-3r_4} \right) 6(\delta^0$$

$$\left. -\gamma)^2(1+\lambda)^2 + Y^0_{CH2D2} \right) e^{-r\tau}$$

$$Y_{CHD3} = \left(-\left(\frac{1}{4}\frac{\left((4\lambda-8)r_4+(\lambda-5)r_3-2r_2\right)(\delta^0-\gamma)(4\gamma-3)e^{-\frac{3}{4}\left((r_1+2r_2+3r_3+4r_4)\lambda-\frac{1}{3}(4r_0+r_1-2r_2-5r_3-8r_4)\right)\tau}}{-\frac{3}{4}(r_1+2r_2+3r_3+4r_4)\lambda+r_0+\frac{1}{4}(r_1-2r_2-5r_3-8r_4)} \right.\right. \quad (5\ A1)$$

$$\left. - \frac{1}{2}\frac{(2\gamma-1)\gamma r''e^{-\frac{1}{2}((r_1+2r_2+3r_3+4r_4)\lambda-2r_0-r_1+r_3+2r_4)\tau}}{-\frac{1}{2}(r_1+2r_2+3r_3+4r_4)\lambda+r_0+\frac{1}{2}(r_1-r_3-2r_4)} \right.$$

$$\left. - \frac{\left((\lambda^2-2\lambda+3)r_4+(-\lambda+2)r_3+r_2\right)(\delta^0-\gamma)^2e^{-((r_1+2r_2+3r_3+4r_4)\lambda-r_0+r_2+2r_3+3r_4)\tau}}{-(r_1+2r_2+3r_3+4r_4)\lambda+r_0-r_2-2r_3-3r_4} \right) 4(\delta^0-\gamma)^2(1+\lambda)^2$$

$$+\left(\frac{1}{4}\frac{\left((4\lambda-8)r_4+(\lambda-5)r_3-2r_2\right)(\delta^0-\gamma)(4\gamma-3)}{-\frac{3}{4}(r_1+2r_2+3r_3+4r_4)\lambda+r_0+\frac{1}{4}(r_1-2r_2-5r_3-8r_4)} \right.$$

$$\left. - \frac{1}{2}\frac{(2\gamma-1)\gamma r''}{-\frac{1}{2}(r_1+2r_2+3r_3+4r_4)\lambda+r_0+\frac{1}{2}(r_1-r_3-2r_4)} - \frac{\left((\lambda^2-2\lambda+3)r_4+(-\lambda+2)r_3+r_2\right)(\delta^0-\gamma)^2}{-(r_1+2r_2+3r_3+4r_4)\lambda+r_0-r_2-2r_3-3r_4} \right) 4(\delta^0$$

$$\left. -\gamma)^2(1+\lambda)^2 + Y^0_{CHD3} \right) e^{-r\tau}$$

$$Y_{CD4} = \left(-\left(\frac{\left((4\lambda-8)r_4+(\lambda-5)r_3-2r_2\right)(\delta^0-\gamma)\gamma e^{-\frac{3}{4}\left((r_1+2r_2+3r_3+4r_4)\lambda-\frac{1}{3}(4r_0+r_1-2r_2-5r_3-8r_4)\right)\tau}}{-\frac{3}{4}(r_1+2r_2+3r_3+4r_4)\lambda+r_0+\frac{1}{4}(r_1-2r_2-5r_3-8r_4)} \right.\right. \quad (6\ A1)$$

$$\left. - \frac{\gamma^2r''e^{-\frac{1}{2}((r_1+2r_2+3r_3+4r_4)\lambda-2r_0-r_1+r_3+2r_4)\tau}}{-\frac{1}{2}(r_1+2r_2+3r_3+4r_4)\lambda+r_0+\frac{1}{2}(r_1-r_3-2r_4)} \right.$$

$$\left. - \frac{\left((\lambda^2-2\lambda+3)r_4+(-\lambda+2)r_3+r_2\right)(\delta^0-\gamma)^2e^{-((r_1+2r_2+3r_3+4r_4)\lambda-r_0+r_2+2r_3+3r_4)\tau}}{-(r_1+2r_2+3r_3+4r_4)\lambda+r_0-r_2-2r_3-3r_4} \right) (\delta^0-\gamma)^2(1+\lambda)^2$$

$$+\left(\frac{\left((4\lambda-8)r_4+(\lambda-5)r_3-2r_2\right)(\delta^0-\gamma)\gamma}{-\frac{3}{4}(r_1+2r_2+3r_3+4r_4)\lambda+r_0+\frac{1}{4}(r_1-2r_2-5r_3-8r_4)} - \frac{\gamma^2r''}{-\frac{1}{2}(r_1+2r_2+3r_3+4r_4)\lambda+r_0+\frac{1}{2}(r_1-r_3-2r_4)} \right.$$

$$\left. - \frac{\left((\lambda^2-2\lambda+3)r_4+(-\lambda+2)r_3+r_2\right)(\delta^0-\gamma)^2}{-(r_1+2r_2+3r_3+4r_4)\lambda+r_0-r_2-2r_3-3r_4} \right) (\delta^0-\gamma)^2(1+\lambda)^2 + Y^0_{CD4} \Bigg)$$

It should be noted that the obtained equations can only be used for the description of hydrogen isotope redistribution between the gas phase and a powder sample, on account of the exponential kinetic model used when obtaining the equations. In the case of ceramics or monocrystal samples, the diffusion equations have to be used.

Each equation has to be described by the same parameters. Thus, simultaneous fitting of six curves has to be carried out in order to describe all dependencies with the same values of r_0, r_1, r_2, r_3, and r_4 types of exchange.

2. Two-step methane activation mechanism

A similar approach can be used for the two-step methane activation mechanism equations (32)–(36). The exponential kinetic model equation in this case can be presented as (7 A1), taking into account equations (29) and (31).

$$\delta = \gamma + (\delta^0-\gamma)e^{-r_a p(1+\lambda)\tau}. \quad (7\ A1)$$

Kinetic equations (32)–(36), as well as equation (18)–(22), are first-order differential equations and can be solved in the same way as that described above. The analytic solutions for these equations can be presented as the following:

$$Y_{CH4} = \left(\left(-\frac{(6+(1+\lambda)^2p^2+(-4\lambda-4)p)(\delta^0-\gamma)^2e^{-r_a(4\lambda p+4p-1)\tau}}{r_a(4\lambda p+4p-1)} + (2-2\gamma)\left(-\frac{2\big((1+\lambda)p-3\big)(\delta^0-\gamma)e^{-r_a(3\lambda p+3p-1)\tau}}{r_a(3\lambda p+3p-1)} - \frac{(3-3\gamma)e^{-r_a(2\lambda p+2p-1)\tau}}{r_a(2\lambda p+2p-1)}\right)\right)p^2r_a(\delta^0-\gamma)^2(1+\lambda)^2 - \left(-\frac{(6+(1+\lambda)^2p^2+(-4\lambda-4)p)(\delta^0-\gamma)^2}{r_a(4\lambda p+4p-1)} + (2-2\gamma)\left(-\frac{2\big((1+\lambda)p-3\big)(\delta^0-\gamma)}{r_a(3\lambda p+3p-1)} - \frac{(3-3\gamma)}{r_a(2\lambda p+2p-1)}\right)\right)p^2r_a(\delta^0-\gamma)^2(1+\lambda)^2 + Y^0_{CH4}\right)e^{-r_a\tau} \quad (8\ A1)$$

$$Y_{CH3D} = \left(\left(-\frac{(6+(1+\lambda)^2p^2+(-4\lambda-4)p)(\delta^0-\gamma)^2e^{-r_a(4\lambda p+4p-1)\tau}}{r_a(4\lambda p+4p-1)} + \frac{\big((1+\lambda)p-3\big)(\delta^0-\gamma)(4\gamma-3)e^{-r_a(3\lambda p+3p-1)\tau}}{r_a(3\lambda p+3p-1)} - \frac{(6\gamma^2-9\gamma+3)e^{-r_a(2\lambda p+2p-1)\tau}}{r_a(2\lambda p+2p-1)}\right)4p^2r_a(\delta^0-\gamma)^2(1+\lambda)^2 - \left(-\frac{(6+(1+\lambda)^2p^2+(-4\lambda-4)p)(\delta^0-\gamma)^2}{r_a(4\lambda p+4p-1)} + \frac{\big((1+\lambda)p-3\big)(\delta^0-\gamma)(4\gamma-3)}{r_a(3\lambda p+3p-1)} - \frac{(6\gamma^2-9\gamma+3)}{r_a(2\lambda p+2p-1)}\right)4p^2r_a(\delta^0-\gamma)^2(1+\lambda)^2 + Y^0_{CH3D}\right)e^{-r_a\tau} \quad (9\ A1)$$

$$Y_{CH2D2} = \left(\left(-\frac{(6+(1+\lambda)^2p^2+(-4\lambda-4)p)(\delta^0-\gamma)^2e^{-r_a(4\lambda p+4p-1)\tau}}{r_a(4\lambda p+4p-1)} + \frac{2\big((1+\lambda)p-3\big)(\delta^0-\gamma)(2\gamma-1)e^{-r_a(3\lambda p+3p-1)\tau}}{r_a(3\lambda p+3p-1)} - \frac{(6\gamma^2-6\gamma+1)e^{-r_a(2\lambda p+2p-1)\tau}}{r_a(2\lambda p+2p-1)}\right)6p^2r_a(\delta^0-\gamma)^2(1+\lambda)^2 - \left(-\frac{(6+(1+\lambda)^2p^2+(-4\lambda-4)p)(\delta^0-\gamma)^2}{r_a(4\lambda p+4p-1)} + \frac{2\big((1+\lambda)p-3\big)(\delta^0-\gamma)(2\gamma-1)}{r_a(3\lambda p+3p-1)} - \frac{(6\gamma^2-6\gamma+1)}{r_a(2\lambda p+2p-1)}\right)6p^2r_a(\delta^0-\gamma)^2(1+\lambda)^2 + Y^0_{CH2D2}\right)e^{-r_a\tau} \quad (10\ A1)$$

$$Y_{CHD3} = \left(-\left(\frac{(6+(1+\lambda)^2p^2+(-4\lambda-4)p)(\delta^0-\gamma)^2e^{-r_a(4\lambda p+4p-1)\tau}}{r_a(4\lambda p+4p-1)} - \frac{\big((1+\lambda)p-3\big)(\delta^0-\gamma)(4\gamma-1)e^{-r_a(3\lambda p+3p-1)\tau}}{r_a(3\lambda p+3p-1)} + \frac{3(2\gamma-1)\gamma e^{-r_a(2\lambda p+2p-1)\tau}}{r_a(2\lambda p+2p-1)}\right)4p^2r_a(\delta^0-\gamma)^2(1+\lambda)^2 + \left(\frac{(6+(1+\lambda)^2p^2+(-4\lambda-4)p)(\delta^0-\gamma)^2}{r_a(4\lambda p+4p-1)} - \frac{\big((1+\lambda)p-3\big)(\delta^0-\gamma)(4\gamma-1)}{r_a(3\lambda p+3p-1)} + \frac{3(2\gamma-1)\gamma}{r_a(2\lambda p+2p-1)}\right)4p^2r_a(\delta^0-\gamma)^2(1+\lambda)^2 + Y^0_{CHD3}\right)e^{-r_a\tau} \quad (11\ A1)$$

$$Y_{CD4} = \left(\left(-\frac{(6+(1+\lambda)^2p^2+(-4\lambda-4)p)(\delta^0-\gamma)^2e^{-r_a(4\lambda p+4p-1)\tau}}{r_a(4\lambda p+4p-1)} + \frac{\big((1+\lambda)p-3\big)(\delta^0-\gamma)2\gamma e^{-r_a(3\lambda p+3p-1)\tau}}{r_a(3\lambda p+3p-1)} - \frac{6\gamma^2e^{-r_a(2\lambda p+2p-1)\tau}}{r_a(2\lambda p+2p-1)}\right)p^2r_a(\delta^0-\gamma)^2(1+\lambda)^2 - \left(-\frac{(6+(1+\lambda)^2p^2+(-4\lambda-4)p)(\delta^0-\gamma)^2}{r_a(4\lambda p+4p-1)} + \frac{\big((1+\lambda)p-3\big)(\delta^0-\gamma)2\gamma}{r_a(3\lambda p+3p-1)} - \frac{6\gamma^2}{r_a(2\lambda p+2p-1)}\right)p^2r_a(\delta^0-\gamma)^2(1+\lambda)^2 + Y^0_{CD4}\right)e^{-r_a\tau} \quad (12\ A1)$$

where p is the probability of hydrogen incorporation, calculated from eq. (37), and r_a is the dissociative adsorption rate. Equations (8 A1)–(12 A2) are similar to equations (2 A1)–(6 A2); however, in the case of the two-step methane activation mechanism equations, we only have two independent parameters, i.e., r_a and p. Thus, the two-step methane activation mechanism is a particular case of the general five types of H/D exchange model.

In order to find the constraints (38)–(41) presented in the main part of the article, we should match the five types of exchange from the mechanistic model with the dissociative adsorption rate and the probability of the hydrogen incorporation process from the two-step methane activation mechanism. These expressions can be written as the following:

$$r = r_a, \quad (13\ A1)$$
$$r_H = r_a p, \quad (14\ A1)$$
$$r_0 = r_a(1-p)^4, \quad (15\ A1)$$
$$r_1 = 4r_a p(1-p)^3, \quad (16\ A1)$$
$$r_2 = 6r_a p^2(1-p)^2, \quad (17\ A1)$$
$$r_3 = 4r_a p^3(1-p), \quad (18\ A1)$$
$$r_4 = 4r_a p^4. \quad (19\ A1)$$

By combining equations (15 A1) and (19 A1), one can obtain constraints equations (38)–(41).

Appendix 2

Experiment of H/D isotopic exchange between CH_4 and proton-conducting oxide

1. Set-up scheme

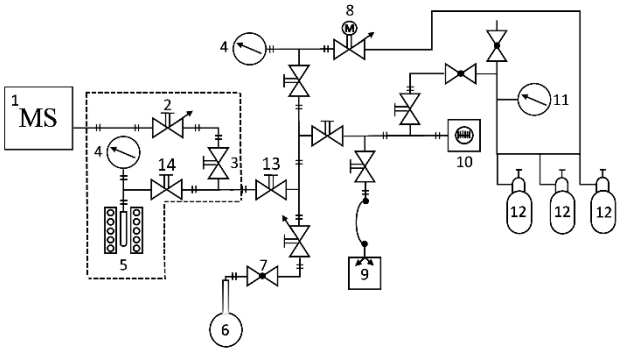

Figure 1. The experimental set-up scheme for the methane isotopic exchange: 1) mass-spectrometer Microvision 2 Vision 2000 P; 2) leakage valve with manual adjustment; 3) T-type vacuum valve (Agilent); 4) Bayard-Alpert-Pirani pressure transducer FRG-720; 5) quartz reactor with a sample; 6) round-bottomed flask with CD_4 gas; 7) vacuum valve; 8) leakage valve with electrical adjustment; 9) spiral pump IDK-2; 10) vacuum system MiniTask AG 81; 11) high-pressure transducer; 12) gas cylinder filled with H_2, D_2, and CH_4 gases. The gas circuit was made from Swagelok stainless steel tubes.

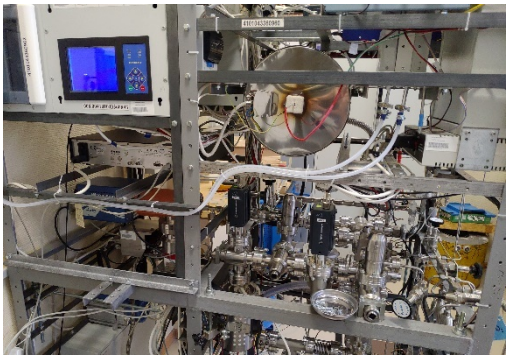

Figure 2. The image of the experimental set-up for the in situ isotopic exchange experiments with gas-phase equilibration in the laboratory.

2. Experiment with a reactor without a specimen

In order to check the possibility of H/D scrambling between methane and the quartz reactor (number 5 in **Figure 1**), an isotopic exchange experiment with a reactor without a specimen was conducted. In the beginning, the reactor was heated to 573 K under vacuum conditions of 10^{-6} mbar. Next, 5 mbar of CH_4 (volume fraction of 99.999%; $H_2O < 10^{-4}$ %) was added to the reactor chamber (number 5 in **Figure 1**). The reactor chamber with CH_4 was closed from the other parts of the gas circuit by a T-type valve (number 3 in **Figure 1**). The gas circuit, except for the reactor chamber, was repeatedly evacuated, followed by the addition of 5 mbar of CD_4 (CD_4 mass fraction of 99%; H_2 mass fraction of 1%; isotopic purity of 99.3%) into the gas circuit using a diamond leakage valve (number 2 in **Figure 1**). The beginning of the experiment was assumed to be when the reactor chamber T-valve was opened. The reactor with the 1:1 CH_4/CD_4 gas mixture was sustained at 573 K for 15 minutes, followed by linear heating to 1073 K at a rate 100 K/h. The experiment was finished after 15 minutes of exposure at 1073 K. **Figure 3** and **Figure 4** represents the results of the experiment with the reactor without a specimen. The obtained results clearly indicate the absence

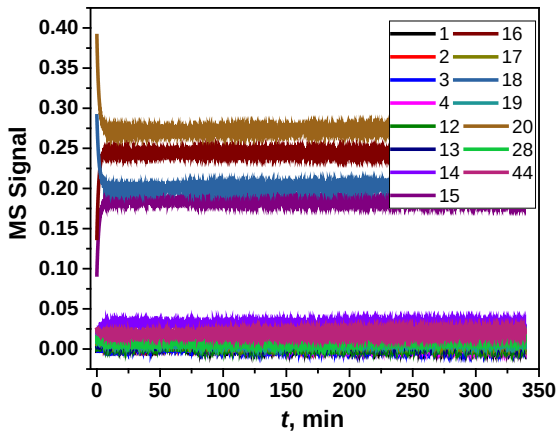

Figure 3. The time dependencies of MS Signal for CH_4/CD_4 isotopic exchange experiment with the reactor without a sample obtained at a total pressure of 5 mbar of mixture 1:1 CH_4:CD_4 in the range 573 – 1223 K.

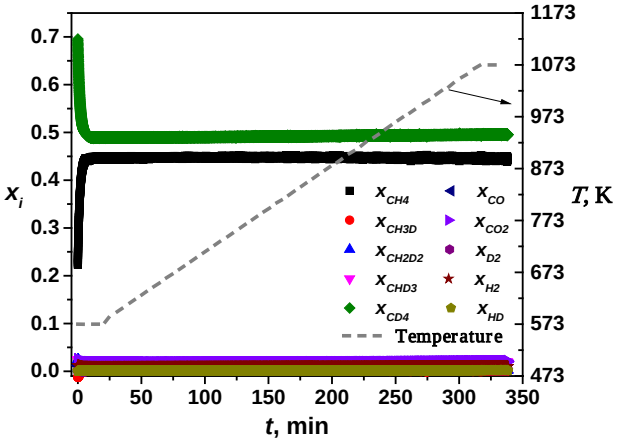

Figure 4. The time dependencies of gas molecule fractions in CH_4/CD_4 isotopic exchange experiment with the reactor without a sample obtained at a total pressure of 5 mbar of mixture 1:1 CH_4:CD_4 in the range 573 – 1223 K.

of any isotopic redistribution processes in the reactor without a specimen. The raw data obtained in the experiment can be recalculated in the gas molecule fractions using the artificial neural network described in Appendix 3.

Appendix 3

Calculation of gas phase molecule fractions

1. Defining the structure of the artificial neural network

The separation of methane isotopic forms (CH_4, CH_3D, CH_2D_2, CHD_3, CD_4) in mass spectrometry is a well-known problem[1–3]. On account of ionisation, each methane isotopomer molecule is destroyed in the mass spectrometer camera, forming numerous different fragments, i.e., CX_4 (X is H or D), CX_3, CX_2, CX, C, and CX_5^+. Basic fragments for all methane isotopomers are listed in **Table 1**. One can see that almost all mass spectra of methane isotopomers overlap. The possible presence of carbon monoxide, carbon dioxide, and hydrogen isotopomers also creates additional problems for distinguishing spectra. One possible way to quantitatively recalculate the mass spectra into the gas phase molecule concentration is to use a mathematical algorithm called an artificial neural network.

Table 1. Basic methane isotopomers fragments obtained in mass-spectrometer during the ionization process

Mass number, m/z	Methane isotopomers fragments				
	CH_4	CH_3D	CH_2D_2	CHD_3	CD_4
12	C	C	C	C	C
13	CH	CH	CH	CH	–
14	CH_2	CH_2, CD	CH_2, CD	CD	CD
15	CH_3	CH_3, CHD	CHD	CHD	–
16	CH_4	CD_2, CH_2D, CH_3	CD_2, CH_2D,	CD_2	CD_2
17	–	CH_3D,	CHD_2	CHD_2	–
18	–	–	CH_2D_2	CD_3	CD_3
19	–	–	–	CD_3H	–
20	–	–	–	–	CD_4

The two-layered feed-forward artificial neural network was created using Matlab software. A graphical scheme of the neural network is presented in **Figure 5**. According to **Figure 5**, an 'input' on the scheme is a vector column containing the intensity of 15 mass signals normalised to the range 0 – 1. An 'output' represents the vector column containing 10 elements representing the fraction of 10 gas molecules. Each hidden and output neuron in the network can be represented with the expressions (1 3A)–(3 3A), as follows:

$$H_i = \frac{e^z - e^{-z}}{e^z + e^{-z}} \quad (1\ 3A)$$

$$z_i = \sum_{j=1}^{15} w_j \cdot I_j^{rel} + b_i, \quad (2\ 3A)$$

$$O_n = \sum_{l=1}^{50} w_l \cdot H_l + b_n, \quad (3\ 3A)$$

where H_i represents the value of the *i*-th hidden neuron; w_j and b_i are weights of the *i*-th hidden neuron; O_n represents the value of the *n*-th output neuron and corresponds to the fraction of *n*-th type molecule in the gas phase;; and w_l and $b_n$are the weights of the *n*-th output neuron.

In order to train the artificial neural network, an appropriate training data set should be created. However, if the training data set is created using only mixtures manually created in the set-up, the number of possible instances will be not sufficient to achieve good agreement between the raw data and the actual gas molecule concentration. Thus, it is necessarily to create a training set mathematically using known spectra of individual substances.

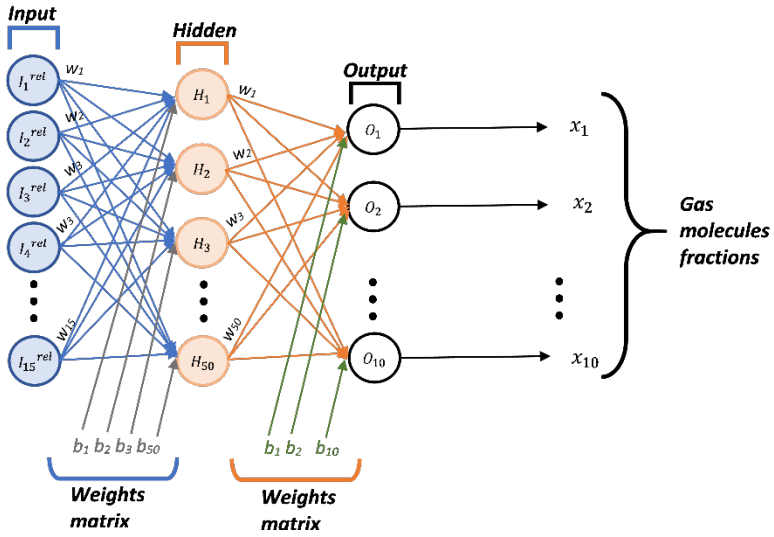

Figure 5. The graphical scheme of the two-layered artificial neural network created for the calculation of gas molecules fractions (CH_4, CH_3D, CH_2D_2, CHD_3, CD_4, H_2, D_2, HD, CO, CO_2) in the mixture CH_4:H_2:CD_4 9:1:10.

2. Training set

The training set was generated using the known mass spectra of different gas molecules, taking into account changes in ionic currents of different mass signals with total pressure. The process of creating the training data set was done in several steps. In the first step, the raw spectra of single gases were measured for H_2, D_2, CH_4, CD_4, CO and CO_2. In order to exclude the influence of pressure on the data, the obtained spectra intensity was normalised by eq. (4 3A)–(5 3A), as follows

$$I_j^{rel} = \frac{I_j}{\sum_{j=1}^{15} I_j}, \tag{4 3A}$$

$$\sum_{j=1}^{15} I_j^{rel} = 1, \tag{5 3A}$$

where I_j^{rel} is the related intensity of the *j*-th mass number and I_j is the measured absolute intensity. The mass spectra of CH_3D, CH_2D_2, and CHD_3 were linearly recalculated from the literature data[1] on account of the extremely close match between the mass number ratios in the literature and our spectra for pure gases (see **Table 2**).

Table 2. Comparison of the literature[1] mass spectra for CH_4 and the measured CH_4 spectra in present work.

Mass number	Related intensity $I_j^{rel} = \frac{I_j}{I_{max}}$	
	CH_4	CH_4[1]
12	0.0068	0.0107
13	0.0276	0.0284
14	0.1296	0.0791
15	0.7920	0.796
16	1	1

On account of the systematic error of the mass spectrometer, the value of intensity for each mass number can vary within some limits. In this case, the related intensity can also have different values. To train the artificial neural network, this error has to be taken into account. To do this, we calculated the average and standard deviation for each mass number of each molecule in the gas phase. Then, the mass spectra of each molecule were reconstructed with the assumption that the error of the measurements met the normal distribution law. For each gas phase molecule, 7000 instances of pure spectra were generated.

In the second step, the 500 target values were created, representing the different mixture compositions of 10 gas phase molecules. The gas molecule concentration has to be restricted with equation (6 3A), as follows:

$$1 = \sum_k x_k, \tag{6 3A}$$

where k resents different types of gas phase molecules (H_2, D_2, HD, CH_4, CH_3D, CH_2D_2, CHD_3, CD_4, CO, CO_2).

The Input training set was generated from target values, taking into account that the intensity of the *i*-th mass number is a sum of contributions of different fragments from different gas molecules, e. g., mass number 16 is a sum of the contribution of CH_4 from CH_4, CH_2D from CH_3D and CH_2D_2, CD_2 from CD_4, CH_2D_2 and CHD_3, and O from CO and CO_2. In this case, the related intensity for each mass number can be represented with equation (7 3A), as follows:

$$I_j^{rel} = \sum_k x_k \cdot \frac{I_j^k}{\sum_{j=1}^{15} I_j^k}, \tag{7 3A}$$

The overall training data set included about $3.6 \cdot 10^6$ instances. Each example represents 7000 mass spectra variants for a particular gas phase mixture. The process of artificial neural network training was done according to the conventional back propagation algorithm with the Bayesian regularisation method[4,5]. The Bayesian regularisation algorithm was used on account of its benefits related to problem with noisy data fitting[4,5]. The change in mean square error during the training procedure is presented in **Figure 6**, where the epoch corresponds to the number of current training iterations and the circle represents the best training performance. The distribution of the neural network error after training is shown in **Figure 7**. As can be seen from the figure, most of the output values have an error of 0.1%. For some points that represent the lowest fraction values, the error level can be 1.4 These results show that for small gas phase molecule concentrations, the value of the mass spectrometer error makes it difficult to calculate the exact value of the concentration.

In order to test the performance of the artificial neural network with the experimentally obtained data, mixtures of CH_4/CD_4 with different ratios of the basic components were created in the gas circuit. The other test was the analysis of CD_4 gas cylinder enrichment with deuterium. The results of the tests are summarised in **Table 3** and **Table 4**. According to **Table 3**, the error level for the major component of the mixture is in the range of 1–6%, while the error was 10–15% for the minor mixture component.

In the case of calculation of deuterium enrichment in the CD_4 cylinder (see **Table 4**), the error was 2.5%. The results show that the artificial neural network is able to recalculate raw data signals into the gas phase molecule fractions, with good agreement.

However, for some points that were related by a small concentration of CH_4 or CD_4 (mixture numbers 7 and 8), high error values (23% and 42%) could be observed. These results can be understood with respect to **Figure 7**. This figure shows that most of the training points (about $3.6 \cdot 10^6$) are located in the error range of –0.2 to 0.2%; however, few points (about 10^2 to 10^3) can significantly deviate from this error. For real experimental data, this error can be higher. As mentioned above, this can occur when the mass signal intensities for a small concentration of gas molecules is significantly less than the systematic error of the mass spectrometer. Thus, if some mass signal intensities, e.g., 13 and 14, at small concentrations of CH_3D and CH_2D_2 are significantly less than the systematic error of the mass spectrometer and the mass signals for the molecules overlap, the error level will be higher.

Table 3. The results of the artificial neural network experimental data fitting in regard to calibration mixtures.

Mixture number	P_i/P_{tot}		Results of artificial neural network calculation	
	X_{CD4}	X_{CH4}	X_{CD4}	X_{CH4}
1	1.00	0.00	0.998±0.002	0,002±0.002
2	0.92	0.08	0.931±0.002	0.069±0.002
3	0.77	0.23	0.794±0.003	0.206±0.003
4	0.50	0.50	0.510±0.004	0.490±0.004
5	0.33	0.67	0.361±0.003	0.639±0.003
6	0.24	0.76	0.278±0.003	0.722±0.003
7	0.16	0.84	0.197±0.002	0.803±0.002
8	0.10	0.90	0.142±0.002	0.958±0.002
9	0.00	1.00	0.000±0.002	1.000±0.002

Table 4. Results of the CD_4 gas cylinder analysis with the artificial neural network.

	Results of artificial neural network calculation		Factory enrichment data, %
	Isotopomer fraction, %	Deuterium enrichment, %	
CD_4	91.0±0.2	96.8±0.2	99.3
CD_3H	6.1±0.2		
CD_2H_2	2.3±0.2		
CDH_3	0.6±0.2		
CH_4	0.0±0.2		

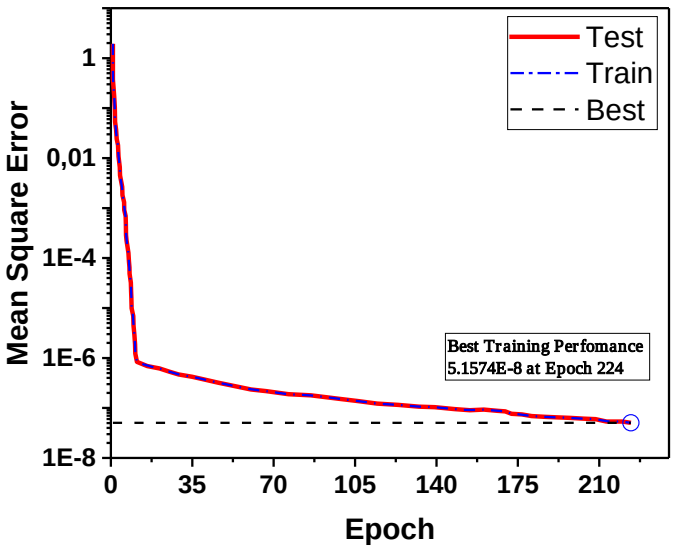

Figure 6. The change of mean square error during the neural network training procedure. 'Train' line represents the part of the training data set used to train the neural network during the training procedure; 'Test' line corresponds to the part of the training set used for the independent test of neural network agreement with the target values (different gas molecules fractions CH_4, CH_3D, CH_2D_2, CHD_3, CD_4, H_2, D_2, HD, CO, CO_2); and 'Best' line represent lowest mean square error.

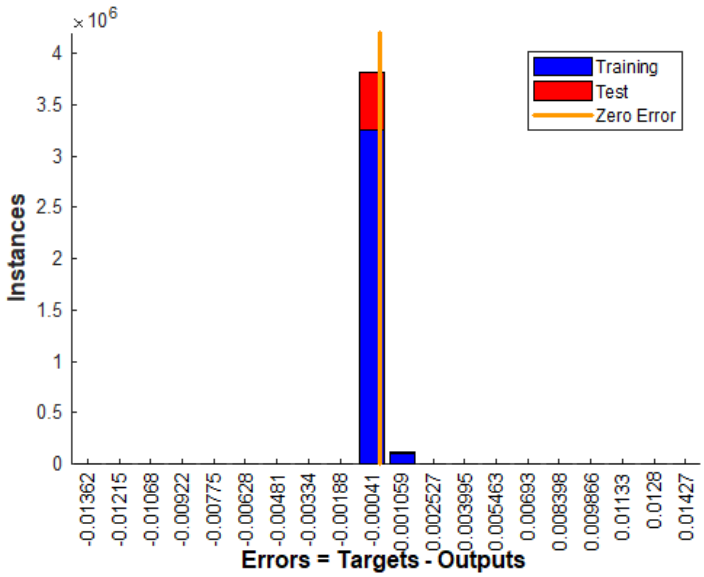

Figure 7. Distribution of the artificial neural network error among the training data set. 'Training' represents the part of the training data set that was used for neural network training, and 'Test' represents the part of the training data set that was used for the neural network test.

Notes and references

1 D.O. Schissler, S.O. Thompson and J. Turkevich. Behaviour of paraffin hydrocarbons on electron impact. *Discuss. Faraday. Soc*. 1951, **10**, 46-53.

2 V.H. Dibeler and F.L. Mohler. Mass Spectra of the Deuteromethanes. *J. Res. Nat. Bur. Stand.* 1950, **45**, 441-444.

3 F.L. Mohler, V.H. Dibeler and E. Quinn. Redetermination of Mass Spectra of Deuteromethanes. *J. Res. Nat. Bur. Stand.* 1958, **61**, 171-172.

4 D. J. C. MacKay. Bayesian interpolation. *Neural comput*. 1992, **4,** 415-447.

5 F. Dan Foresee and M. T. Hagan. Gauss-Newton approximation to Bayesian learning. *IEEE IJCNN.* 1997, **1-4**, 1930-1935.